Food Chemistry: X 22 (2024) 101466

Contents lists available at ScienceDirect

Food Chemistry: X

journal homepage: www.sciencedirect.com/journal/food-chemistry-x

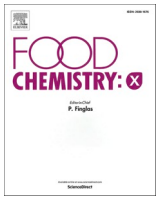

Binary hydrogels constructed from lotus rhizome starch and different types of carrageenan for dysphagia management: Nonlinear rheological behaviors and structural characteristics

Xin-Yu Jiang, Lin Li, Jia-Nan Yan, Ce Wang, Bin Lai *, Hai-Tao Wu *

SKL of Marine Food Processing & Safety Control, National Engineering Research Center of Seafood, Collaborative Innovation Center of Seafood Deep Processing, School of Food Science and Technology, Dalian Polytechnic University, Dalian 116034, China

ARTICLE INFO

Keywords:
Lotus rhizome starch
Carrageenan
Binary hydrogel
Structural characteristics
Nonlinear rheological behaviors
Dysphagia management

Chemical compounds studied in this article:
κ-carrageenan (PubChem CID: 73155740)
ι-carrageenan (PubChem CID: 73155736)
λ-carrageenan (PubChem CID: 91972149)

ABSTRACT

This study focused on binary hydrogels constructed from lotus rhizome starch (LRS) and three types of carrageenan (κ-C, ι-C, and λ-C). The enthalpy of LRS gelatinization was reduced by 32.1%-88.4% with the incorporation of carrageenan. Compared with ι-C and λ-C, the conformations of κ-C more facilitated the development of the binary hydrogel network structure. The ability of the LRS/carrageenan binary hydrogel to immobilize water was mainly related to the effect of different types of carrageenan on starch molecular ordering. LRS-based hydrogels were recognized as level 4 in the International Dysphagia Diet Standardization Initiative (IDDSI) framework. Nevertheless, the incorporation of carrageenan significantly reduced the ability of the LRS hydrogel to resist stress under large deformations, which might be favorable to oral processing and swallowing. This research provides preliminary evidence for relevant industries to use carrageenan to adjust LRS hydrogel properties and improve the quality of starch-based foods for dysphagia management.

1. Introduction

Lotus (*Nelumbo nucifera* Gaertn.) is an aquatic dicotyledonous flowering plant native to the Asian continent, occupying an important position in the world due to its numerous purposes. Generally, lotus rhizome can be eaten as a nutrient-rich and fresh tissue vegetable, providing considerable health benefits. Lotus rhizome starch (LRS) is developed from lotus rhizomes by traditional processes such as refining, settling and drying, as a traditional dietary supplement with distinct Chinese characteristics. LRS is consumed mainly as a dessert in China and is especially beneficial to the health of teenagers and seniors (Zhong, Chen, & We, 2007). In addition to starch as the main ingredient, LRS also contains a small amount of protein, lipids, and minerals such as calcium and iron (Jiang et al., 2023). LRS is gluten-free and has unique characteristics. Typical LRS granules exhibit elongated rod-like shapes with long axes of 10–50 μm and short axes of 10–35 μm, which can be gelatinized in the aqueous phase to form a hydrogel matrix with a continuous network structure (Zhu, 2017; Jiang et al., 2023). Gelatinized LRS has been considered for use in clinical nursing and as adjuvant of medication swallowing for patients with dysphagia. However, the hydrogel strength of a single LRS is lower, and its nonlinear viscoelastic properties under large deformations are not clear (Zhu, 2017). Therefore, it is necessary to better understand the nonlinear rheological behavior of LRS hydrogels and modify their hydrogel properties for easier swallowing.

In recent years, the addition of nonstarch polysaccharides has been recognized as an environmentally friendly and effective physical modification method for improving the gelation properties of starch. Typically, the binary combination strategy for starch/polysaccharide hydrogels could compensate for the deficiencies of individual components (Liu, Zhu, Zhong, Yokoyama, Huang, & Li, 2021). For example, the polysaccharide *Mesona chinensis* could reduce the endothermic enthalpy and free water migration of maize starch gel (Luo, Han, Shen, Yang, Ren, & Xie, 2021). Due to the diversity of polysaccharide sources and

Abbreviations: LRS, lotus rhizome starch; κ-C, κ-carrageenan; ι-C, ι- carrageenan; λ-C, λ-carrageenan; IDDSI, International Dysphagia Diet Standardization Initiative; cryo-SEM, cryo-scanning electron microscopy; LVR, linear viscoelastic region; LAOS, large amplitude oscillatory shear; LF-NMR, low-field nuclear magnetic resonance; T_2, transverse spin–spin; MRI, magnetic resonance imaging; DSC, differential scanning calorimetry; XRD, X-ray diffraction; FTIR, Fourier transform infrared.

* Corresponding authors.
E-mail addresses: bin.lai33@gmail.com (B. Lai), wht205@163.com (H.-T. Wu).

https://doi.org/10.1016/j.fochx.2024.101466
Received 10 March 2024; Received in revised form 7 May 2024; Accepted 10 May 2024
Available online 15 May 2024

structures as well as interactions with different starches, these systems remain an open field of research. Carrageenan is a family of anionic linear sulfated polysaccharides extracted from red seaweed that are commonly used in thickening, gelation, and emulsification in food manufacturing. From meat and dairy products to baby foods, carrageenan is preferred in many food products (Gürkan Polat, Duman, & Tunç, 2020). Ideally, carrageenan consists of repeating disaccharide units of α-1,3-linked β-D- galactopyranose and β-1,4-linked 3,6-anhydro-α-D-galactopyranose (Necas & Bartosikova, 2013). Currently, the three major commercial types are kappa-carrageenan (κ-C), iota-carrageenan (ι-C), and lambda-carrageenan (λ-C) (Matignon, Barey, Desprairies, Mauduit, Sieffermann, & Michon, 2014). The κ-C and ι-C undergo a coil-to-helix transition depending on the temperature and ionic environment, whereas λ-C cannot gel due to the absence of anhydrobridges and additional sulfate groups (Huc et al., 2014; Rochas, Rinaudo, & Vincendon, 1980). During starch gelatinization, carrageenan was found to be a protector for starch granules and was highly dependent on the carrageenan type (Lascombes et al., 2017). As previously reported, the viscoelasticity and storage stability of starch gels were significantly improved with the addition of κ-C (Lin, Liang, & Chang, 2016; Liu et al., 2021; Song et al., 2024). Different types of carrageenan may have a specific effect on the gel properties of starch. For example, the dynamic rheological values of rice starch increased according to carrageenan addition in the order λ-C > ι-C > κ-C (Kim, Patel, & BeMiller, 2013). Typically, the properties of starch/polysaccharide mixed gels are determined by specific combinations. For LRS with characteristically large granules, low-methoxy pectin and high-methoxy pectin had distinct effects on partial pasting properties and rheological behaviors, and the changes in adhesion and elasticity of the mixture were related to the pectin type (Zheng, Liu, Zhang, Kan, & Zhang, 2019). Soybean soluble polysaccharide reduced the peak viscosity of LRS and improved the stability of LRS gel, but it led to increased freeze–thaw syneresis and decreased gel hardness (Liu, Li, Fan, Zhang, & Zhong, 2019). The addition of bamboo shoot polysaccharides could inhibit the gelatinization and viscoelasticity of LRS (Zheng et al., 2024). To date, the properties of binary hydrogels constructed from LRS and different types of carrageenan, particularly their rheological behaviors in the nonlinear viscoelastic region and their structural principles, are still unclear. Therefore, understanding the characteristics and advantages of LRS/carrageenan binary hydrogels has both theoretical value and application prospects.

Recently, researchers have focused on the possibility of modifying starchy foods by adding polysaccharide hydrocolloids and the feasibility of their complex systems as potential dysphagia foods. The International Dysphagia Diet Standardization Initiative (IDDSI) framework provides levels of drinks and foods for dysphagia management (Cichero et al., 2017). The addition of soluble soybean polysaccharide could effectively modify the gelatinization and texture of glutinous rice starch, and the 3D-printed Qingtuan met the IDDSI framework level 6 requirements (Kong, Zhang, Mujumdar, & Li, 2023). The addition of Astragalus polysaccharides could modify the texture and network structure of the mung bean starch-flaxseed protein complex gel and make the tripolymeric composite gel system conform to levels 6–7 of the IDDSI framework (Min et al., 2023). However, reports of IDDSI testing for starchy liquid foods with nonstarch polysaccharides are lacking. Researchers have recognized the critical importance of further characterizing the rheological properties of liquid foods to ensure swallowing safety. Furthermore, large amplitude oscillatory shear (LAOS) measurements in the nonlinear region contributed to a deeper understanding of the network development and stress resistance of hydrogel systems (Wang & Selomulya, 2022). It was reported that the characterization of nonlinear viscoelastic behaviors of starch/nonstarch polysaccharide hydrogels by LAOS was helpful to represent more realistic mechanical properties and microstructure (Su, Li, Wang, &Wang, 2023). Therefore, it is necessary to extend the knowledge of the rheological behaviors of LRS/carrageenan hydrogels in the nonlinear viscoelastic region and link them with the IDDSI framework to identify their potential as food for dysphagia management.

This work was designed to investigate and compare the effects of κ-C, ι-C, and λ-C on the visual appearance, microstructure, IDDSI test, linear and nonlinear rheological behaviors, water distribution, thermal properties, and structural characteristics of LRS in binary hydrogel systems. Moreover, this study provided basic information for understanding the network and swallowing characteristics of binary hydrogels constructed from different types of carrageenan and starch with large granules.

2. Materials and methods

2.1. Materials and reagents

The LRS (886.68 g/kg starch content) was obtained from Yunnan Huangnitang Lotus Industry Technology Development Co., Ltd. (Baoshan, China). Three types of carrageenan (κ-C, ι-C, and λ-C) were obtained from Aladdin Co., Ltd (Shanghai, China). The average molecular weights of κ-C, ι-C, and λ-C are 788.7, 946.8, and 579.5 g/mol, respectively.

2.2. Preparation of LRS/carrageenan binary hydrogels

First, κ-C, ι-C, and λ-C powders were dispersed in deionized water, and carrageenan solutions (5.56 mg/mL) were prepared by continuous stirring at 60 °C for 30 min. LRS (50 mg/mL) powders were dispersed in the carrageenan solution to make a suspension and then heated at 95 °C for 30 min. The samples were stirred regularly during the heating process and cooled for 16 h to develop the network structure, and binary hydrogels were prepared.

2.3. Determination of microstructure

The microstructures of the individual LRS and LRS/carrageenan binary hydrogels were photographed via cryo-scanning electron microscopy (cryo-SEM). The samples were pre-frozen and transferred directly to a cryo-SEM preparation chamber under vacuum, fractured, sublimated (−70 °C, 20 min), and sputter-coated (fragile platinum layer), and then examined via a cryo-stage SU8010 scanning electron microscope (Hitachi, Tokyo, Japan).

2.4. IDDSI tests

The IDDSI tests (fork drip test and spoon tilt test) were conducted according to the IDDSI framework to assess the hydrogel samples with IDDSI levels of 3 and 4 (Cichero et al., 2017).

2.5. Determination of rheological behaviors

Oscillatory rheological tests were performed using a rheometer (DHR-2, TA Instruments Ltd., New Castle, USA) equipped with an aluminum parallel plate 40 mm in diameter to collect valuable information about viscoelastic behaviors within the linear viscoelastic region (LVR) and structural changes beyond the LVR at 25 °C. Amplitude oscillatory sweep in the range of 0.01%-1000% strain was performed at 1 Hz with an operation gap of 1 mm. The TRIOS software for rheology advantage data analysis was used for Fourier transform and inverse transformation, and large amplitude oscillatory shear (LAOS) data were collected for analysis. The first strain when the change in the composite modulus was more than 2% of the previous value was recorded as the critical strain, where the stress is recorded as the critical stress (Seighalani, Joyner, & Ross, 2020).

According to the LVR defined by amplitude scanning, a strain of 0.5% was selected for the linear rheological test. The storage modulus (G') and loss modulus (G'') in the frequency range of 0.1–10 Hz, as well as the viscosity in the shear rate range of 0.1–10 Pa·s of the individual

LRS and LRS/carrageenan binary hydrogels, were determined at 25 °C with an operation gap of 1 mm.

2.6. Low-field nuclear magnetic resonance (LF-NMR) measurements

A magnetic resonance analyzer (MesoMR23-060 V-1, Niumag, Suzhou, China) was used to measure the transverse spin–spin (T_2) relaxation of the hydrogen protons in the individual LRS and LRS/carrageenan binary hydrogels. Measurements were processed using the Carr–Purcell–Meiboom–Gill (CPMG) sequence. The main parameter settings included a superposition number (NS) of 4, an echo time (TE) of 0.25 ms, and an echo number (NECH) of 18000. The LF-NMR relaxation curve was fitted to a multiexponential curve, and the peak point time and peak area proportion were obtained.

According to Jiang et al., the LRS and LRS/carrageenan binary hydrogel samples were put into round boxes for magnetic resonance imaging (MRI) (Jiang, Yan, Li, Sun, Nie, & Wu, 2022).

2.7. Differential scanning calorimetry (DSC)

The samples for detecting thermal properties were prepared according to the conditions of LRS/carrageenan binary gels but did not undergo the heating process to reach the gelatinization temperature. The thermal properties of the 40 °C-dried LRS and LRS/carrageenan mixtures were determined by a differential scanning calorimeter (Q2000, TA Instruments, USA). Dried 3 mg and 6 μL of water were added to the sample pan, which was then sealed and left for 12 h to equilibrate. An empty pan served as a reference. The range and rate of temperature increase were 30–100 °C and 10 °C/min, respectively.

2.8. Raman spectroscopy

Raman spectra of vacuum freeze-dried LRS and LRS/carrageenan binary hydrogel samples were obtained using a confocal Raman microscope (Lab RAM HR Evolution, HORIBA, Ltd., Shanghai, China). Spectra with a resolution of 7 cm^{-1} in the range of 3200–100 cm^{-1} were recorded, and the full width at half maximum (FWHM) and relative area of the band at 480 cm^{-1} were calculated (Wang, Sun, Wang, Wang, & Copeland, 2016).

2.9. X-ray diffraction (XRD)

The crystalline patterns of vacuum freeze-dried LRS and LRS/carrageenan binary hydrogel samples were determined by an X-ray diffractometer (XRD-6100, Shimadzu Corporation, Japan). The scanning speed was set at 2 °/min. The variation in the diffraction angle (2 theta) in the range of 3–40° was recorded.

2.10. Fourier transform infrared (FTIR) spectroscopy

Samples of vacuum-freeze-dried LRS and LRS/carrageenan binary hydrogels were subjected to FTIR spectroscopy (PerkinElmer Co. Ltd., USA) for analysis. Spectra were recorded in the range of 4000–400 cm^{-1} with 32 scans and a resolution of 4 cm^{-1}. In the range of 1200–800 cm^{-1}, the FTIR spectra were deconvoluted, Lorentz linear fit, and peak resolved using OMNIC software (Jiang et al., 2023).

2.11. Statistical analysis

Each measurement was performed at least in triplicate, and the data collected in this study were subjected to ANOVA and the Student–Newman–Keuls test to assess the significant differences ($p < 0.05$).

3. Results and discussion

3.1. Visual appearance and microstructure of LRS/carrageenan binary hydrogels

Initially, the visual appearance of LRS/carrageenan binary hydrogels constructed with 50 mg/mL LRS and 5.56 mg/mL κ-C, ι-C, or λ-C is presented in Fig. 1. Compared with that of individual LRS hydrogel with weak fluidity, κ-C, ι-C, and λ-C all contributed to the solid-like behavior of the LRS/carrageenan binary hydrogels. At this concentration, the three types of carrageenan solutions were in a flowing state.

Typically, the gelation properties of a hydrogel are closely related to its network structure. The microstructures of individual LRS hydrogel, LRS/carrageenan binary hydrogels, and three types of carrageenan are presented in Fig. 1. All starch-based hydrogel samples exhibited honeycomb-like network skeleton structures after freezing fracture and low-temperature sublimation in vacuum. As a control, the individual LRS hydrogel showed a relatively dense but thin and fragile skeleton network with very thin pore walls and obvious collapse. For LRS/carrageenan binary hydrogels, relatively smooth and robust cellular networks with thicker pore walls were observed. The looser microscopic network of LRS hydrogels due to the incorporation of carrageenan might be related to the hydrophilicity of polysaccharide molecules allowing more water to be maintained in the network structure of the starch hydrogel, resulting in slightly larger pores after sublimation (Zheng, Huang, Zhao, Wang, Kan, & Zhang, 2021). Similarly, Wei, Ou, Lan, Tang, and Zheng (2023) explained that the changes in the structure of the wheat starch/laminaria polysaccharide system were related to the disruption of crystallization and the reorganization of starch chains during and after heating affected by the addition of polysaccharides. Jia et al. (2023) reported that *Lycium barbarum* polysaccharide induced an irregular network structure of wheat starch, and the microstructure of the mixed gel became looser with increasing polysaccharide content. Moreover, the network structures of the three LRS/carrageenan binary hydrogels were also different, with mesh tidy: LRS/κ-C > LRS/ι-C > LRS/λ-C. Typically, the helical conformation formed by heating leads to the aggregation and gelation of carrageenan molecules, and λ-C exhibits only a thickening effect (Huc et al., 2014; Rochas, Rinaudo, & Vincendon, 1980). The microstructure of three types of carrageenan with the same concentration (0.56 %) confirmed this point (Fig. 1). These results suggested that the presence of carrageenan reduced the interaction between the starch chains but promoted the reorganization and entanglement between carrageenan and starch. The network structural differences of the three LRS/carrageenan binary hydrogels were mainly related to the different molecular conformations of carrageenan.

3.2. Linear viscoelasticity and IDDSI test of LRS/carrageenan binary hydrogels

3.2.1. Dynamic rheological properties

As shown in Fig. 2a, individual LRS hydrogel and LRS/carrageenan binary hydrogels were elastic gels, with G' always exceeding G'' without a crossover within 0.1–10 Hz. The G' and G'' values slightly increased with increasing frequency. A similar phenomenon was observed in the composite systems of rice starch and viscous soluble dietary fibers, which can be classified as typical gels due to their main elastic behavior (Zheng et al., 2021). Accordingly, the hydrogel samples in this work could be considered noncovalently linked gels, which exhibited subtle frequency dependency. In this work, the incorporation of κ-C and ι-C significantly improved the elastic response of the LRS hydrogel, with G' values increasing 1.1-fold and 0.7-fold at 0.1 Hz, respectively. In contrast, the G' and G'' values of LRS/λ-C increased by only 0.2-fold and 0.3-fold, respectively. The possible reason was that the λ-C molecular chains tended to maintain a coil conformation rather than forming helical conformation such as κ-C or ι-C (Schefer, Adamcik, & Mezzenga, 2014). Generally, starch/polysaccharide binary hydrogels mainly

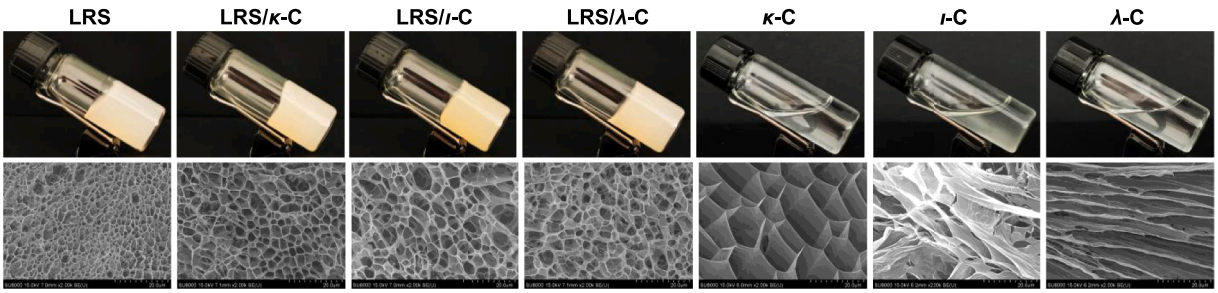

Fig. 1. Visual appearance and cryo-SEM images of LRS/carrageenan binary hydrogels.

involve noncovalent interactions. Similarly, Xie et al. (2021) demonstrated that the main interaction between tapioca starch and *Mesona chinensis* polysaccharide involves hydrogen bonding. Zheng et al. (2021) reported that the addition of viscous soluble polysaccharides enhanced the viscoelastic behaviors of rice starch due to van der Waals forces and hydrogen bonds between polysaccharide chains and amylose. These results suggested that the incorporation of carrageenan resulted in better viscoelasticity of the LRS/carrageenan binary hydrogels, and the synergistic effect of carrageenan on the strength of the LRS hydrogel followed the order of κ-C > ι-C > λ-C. The carrageenan molecular chains might interact with LRS molecules, which further enhances the stability and solid-like behavior of LRS/carrageenan binary hydrogels.

3.2.2. Steady-state flow behaviors

The flow curves of the individual LRS hydrogel and LRS/carrageenan binary hydrogels are presented in Fig. 2b. The viscosity of the samples decreased significantly with shear rates varying from 0.1 to 10 s^{-1}, indicating non-Newtonian shear-thinning behavior. In this case, the incorporation of three types of carrageenan increased the apparent viscosity of LRS. Recent literature reported similar results, such as the promotion of the apparent viscosity of corn starch, potato starch, and lotus seed starch by *Porphyra haitanensis* polysaccharides (Wang, Zhong, Zheng, Zhang, & Zeng, 2023). The intermolecular interaction between starch and polysaccharides could be the reason for the increase in flow resistance and apparent viscosity. In addition, the apparent viscosity of the LRS/carrageenan binary hydrogels exhibited an order of κ-C > ι-C > λ-C at the initial shear rate (data not shown), corresponding to the dynamic rheological properties (Fig. 2a). However, the apparent viscosity of LRS/ι-C decreased sharply as the shear progressed. During the shearing process, the aggregates and entanglements of the molecular chains in the LRS/polysaccharide composite systems were broken and separated, which reduced the shear resistance of the hydrogel samples. Thus, the viscosity order of the three LRS/carrageenan binary hydrogels during shearing might be related to starch molecular ordering. Jia et al. (2023) reported that polysaccharides promoted the formation of ordered starch structures and that the apparent viscosity of sweet potato starch paste decreased with increasing *Lycium barbarum* polysaccharide content. In this case, the stability of LRS/ι-C exhibited a relatively pronounced decrease with increasing shear rate. These results possibly suggested that the steady flow behaviors of the LRS/carrageenan binary hydrogels were more closely related to molecular ordering, while the dynamic rheological properties were more attributable to the conformational characteristics of the carrageenan molecular chains.

3.2.3. IDDSI test results

As a kind of soft food, LRS-based hydrogels might be suitable for the diet management of people with dysphagia. In the IDDSI framework, dysphagia-oriented liquid foods are categorized into five levels (0–4 level) (Cichero et al., 2017). Typically, the weak fluidity of the LRS-based hydrogel prevented it from dropping through the slots of the standard fork in a short period of time (data not shown). Therefore, LRS/carrageenan binary hydrogels and individual LRS hydrogel were recognized as level 4 in this study. The spoon tilt test confirmed this result, as shown in Fig. 2c. Nevertheless, during the spoon tilting process, the LRS/carrageenan binary hydrogels appeared to behave differently from the individual LRS hydrogel in that they were more prone to slipping and flowing down the spoon. Therefore, it was inferred that the presence of carrageenan made the LRS hydrogel more prone to deform, which might be beneficial for reducing the amount of force required for oral processing and swallowing.

3.3. Nonlinear rheological behaviors of LRS/carrageenan binary hydrogels

3.3.1. Oscillatory rheological behaviors

Food often undergoes significant deformation during oral processing. LAOS measurements could provide a richer dimension for analyzing the characteristics and structural differences of food in non-LVR (Duvarci, Yazar, & Kokini, 2017). As shown in Fig. 2d, the values of G' and G'' remained constant with increasing strain when the applied strain was low in the LVR, and when the strain reached a certain value, G' and G'' began to change nonlinearly. The critical strain of both individual LRS and three LRS/carrageenan binary hydrogels was 4.0%. This result showed that the addition of carrageenan did not change the LVR of LRS hydrogel. The stresses of LRS/κ-C, LRS/ι-C, and LRS/λ-C were 9.35, 5.82, and 3.82 Pa, respectively, which were 1.25–3.07 times greater than that of LRS alone. The G' and G'' of LRS hydrogel increased with the addition of three types of carrageenan, and this increase was consistent with the frequency scanning results (Fig. 2a). However, the G' and G'' values of the LRS/carrageenan binary hydrogels changed more sharply beyond the critical strain, which illustrated that the addition of carrageenan made the hydrogel more unstable to oscillation and large-amplitude shear. With increasing strain to non-LVR, the G' of the samples decreased gradually, while the G'' increased slightly at first and then decreased greatly. This phenomenon was interpreted as weak strain overshoot behavior in LAOS, which was a robust feature determined by the equilibrium between the connectivity and damage of hydrogel network structures (Hyun et al., 2011). Therefore, with increasing strain and the continuation of shear, the network structure of the LRS/carrageenan binary hydrogels gradually deteriorated. The loss modulus overshoots of LRS/κ-C and LRS/ι-C were more pronounced than those of the other samples. The networks of the LRS/κ-C and LRS/ι-C hydrogels with higher moduli exhibited greater structural resilience to shear failure. However, the difference between the overshoot behavior of LRS/λ-C and individual LRS was not sufficient to distinguish and explain flow-induced microstructural changes. Therefore, it is necessary to carry out more in-depth qualitative and quantitative analyses on the viscoelastic characteristics in the non-LVR to clarify the differences in the nonlinear stress response of LRS-based hydrogels caused by κ-C, ι-C, and λ-C.

3.3.2. 3D Lissajous curves of the nonlinear rheological behaviors

Lissajous-Bowditch plots provide visual information on complex rheological responses and structural changes under large deformations.

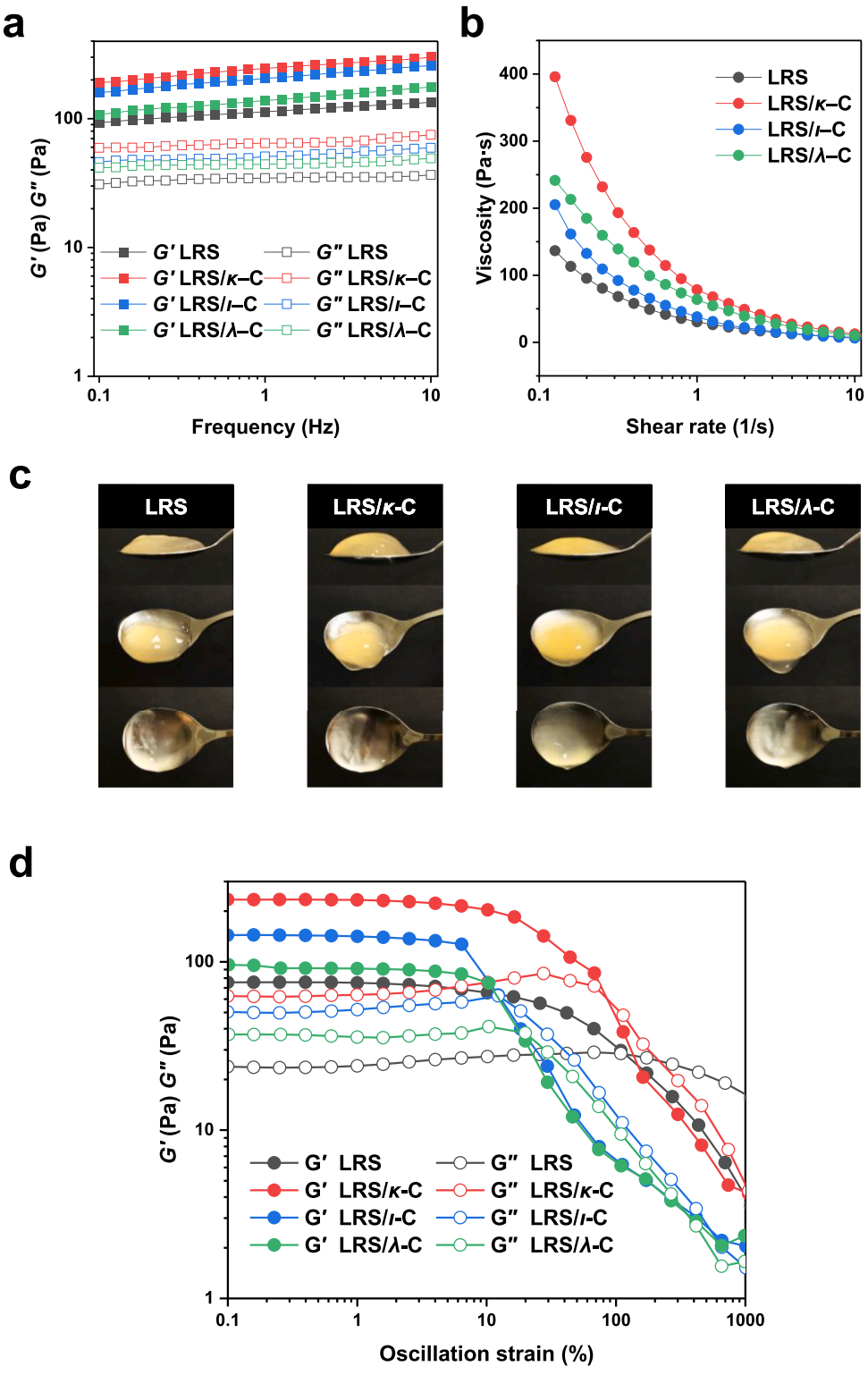

Fig. 2. Dynamic rheological properties (a), steady flow behaviors (b), IDDSI spoon tilt test (c), and changes of storage modulus (G') and loss modulus (G'') in the 0.1%–1000% strain range (d) of LRS/carrageenan binary hydrogels.

The 3D Lissajous curves of the individual LRS and three LRS/carrageenan binary hydrogels in Fig. 3 qualitatively show the viscoelastic variations under LAOS. The projection curves on the stress–strain plane on the right side could be interpreted as an elastic oscillatory response, while the projection curves on the stress–shear rate plane on the left side indicated a viscous response (Ewoldt, Winter, Maxey, & McKinley, 2010). At lower strains, the Lissajous curves exhibited perfect elliptical shapes, which reflected the linear viscoelastic response of the LRS-based hydrogels. As the strain increases further, the closed-loop area of the curve gradually increased and deformation evolved. The closed-loop area of the elastic Lissajous curves is generally consistent with the trend of the unit volumetric energy dissipation of the corresponding

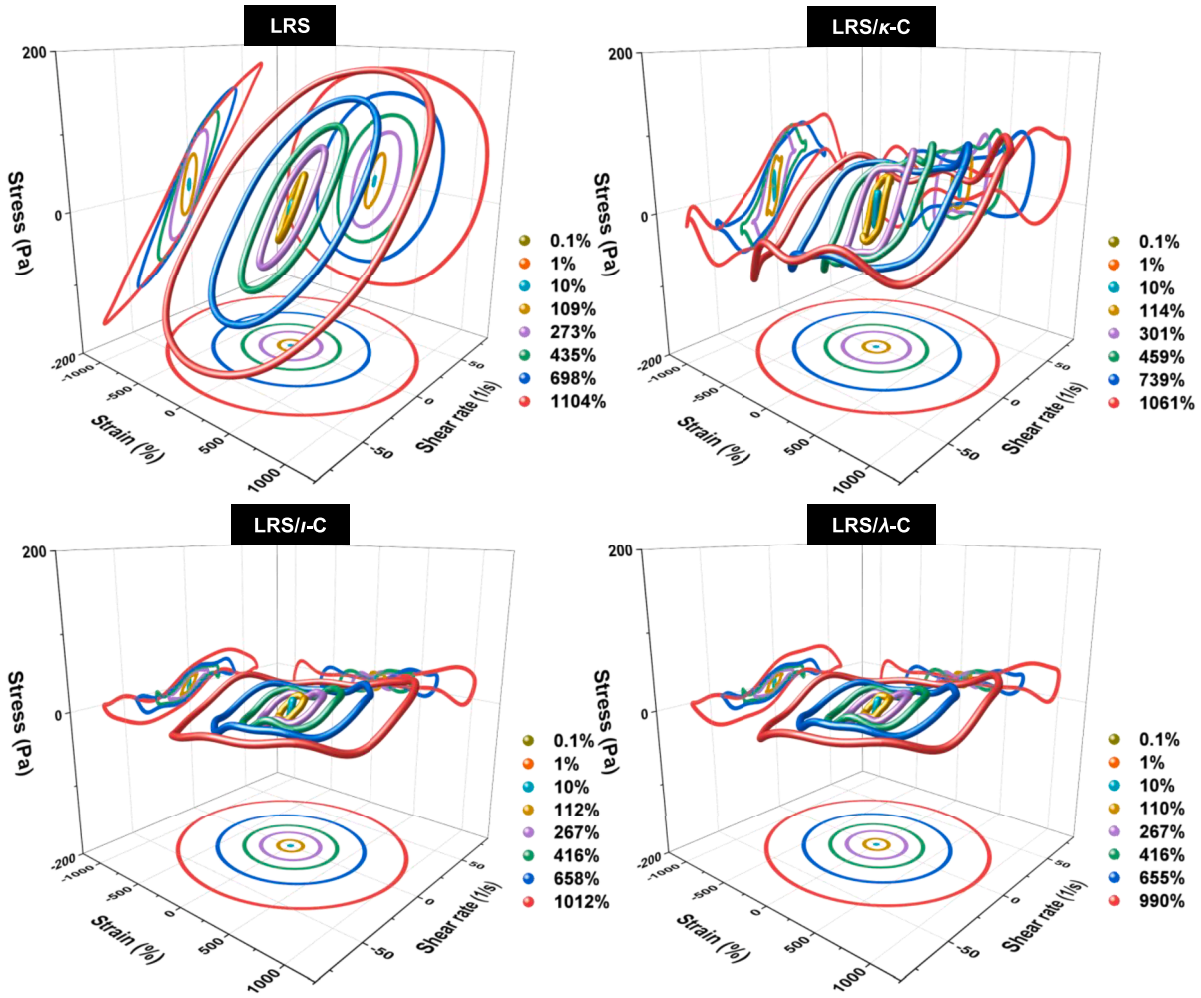

Fig. 3. 3D Lissajous curves of LRS/carrageenan binary hydrogels.

cycle (Duvarci et al., 2017). In contrast, the area surrounded by the Lissajous curve viscous projection indicated the energy stored by the hydrogel network in the corresponding state (Ewoldt, Hosoi, & McKinley, 2008). For individual LRS, the closed-loop area of the viscous response was obviously smaller than that of the elastic response, indicating that the nonlinear rheological behavior gradually became viscous-dominated. The strain-induced stretching of the hydrogel network was released and reversed; in this process, some weak interactions were released, the network became inactive, and the energy stored in the network structure dissipated, leading to more dominant viscous behavior. The major axis of the Lissajous curves rotated clockwise toward the strain axis, indicating that the hydrogel was gradually "softening" (Wang & Selomulya, 2022). LRS/carrageenan binary hydrogels exhibited severe deformation of the Lissajous curves in LAOS, indicating a stronger yield behavior during large deformations. It was suggested that the incorporation of carrageenan reduced the stored energy and energy dissipation of the LRS hydrogel network. The probable reason was that carrageenan incorporation reduced the network structure of energy stored elastically in the hydrogel so that the oscillatory response covered a smaller area than the individual LRS. Furthermore, the binary hydrogels under LAOS exhibited a narrower pattern than the individual LRS hydrogel, indicating that their resistance to stress was significantly reduced (Turksoy, Erturk, Bonilla, Turasan, & Kokini, 2020). The lower stress response of the LRS/carrageenan binary hydrogels under large deformations might suggest that they are easier to orally process and swallow than the individual LRS hydrogel, which was consistent with the results presented in Fig. 2c. Moreover, the network of LRS/κ-C was stronger, corresponding to the results of microstructure characterization (Fig. 1). However, compared with LRS/κ-C, LRS/ι-C and LRS/λ-C exhibited incompletely identical nonlinear behaviors, and the visual appearance of their elastic and viscous projections of 3D Lissajous curves was difficult to distinguish. Therefore, LAOS parameters were needed to further analyze the different effects of κ-C, ι-C, and λ-C on the nonlinear rheological behaviors of LRS hydrogels.

3.3.3. *Fourier transform rheological parameters of the nonlinear rheological behaviors*

Fourier transform rheology and stress decomposition methods were used to obtain more information on the deformation resistance of the samples and to quantitatively evaluate the behaviors of the LRS/carrageenan binary hydrogels under LAOS. The Fourier transform coupled with the Chebyshev polynomials method can be used to compare the relative magnitudes of the elastic and viscous components to capture the local elastoviscous responses of a material under large and small instantaneous strains (Wang & Selomulya, 2022). As shown in Fig. 4a and b, G'_L represents the large strain modulus at the maximum instantaneous strain within each oscillation cycle, and G'_M represents the minimum strain modulus at zero instantaneous strain (Ewoldt et al., 2008). Typically, G'_L and G'_M converged to the linear elastic modulus in the LVR but exhibited differences beyond the LVR. When the oscillating strain increased to approximately 4%, the G'_L and G'_M of the LRS/carrageenan binary hydrogels and individual LRS hydrogel started to decrease, indicating the beginning of a nonlinear transformation. With increasing strain, the G'_L and G'_M of the binary hydrogel samples

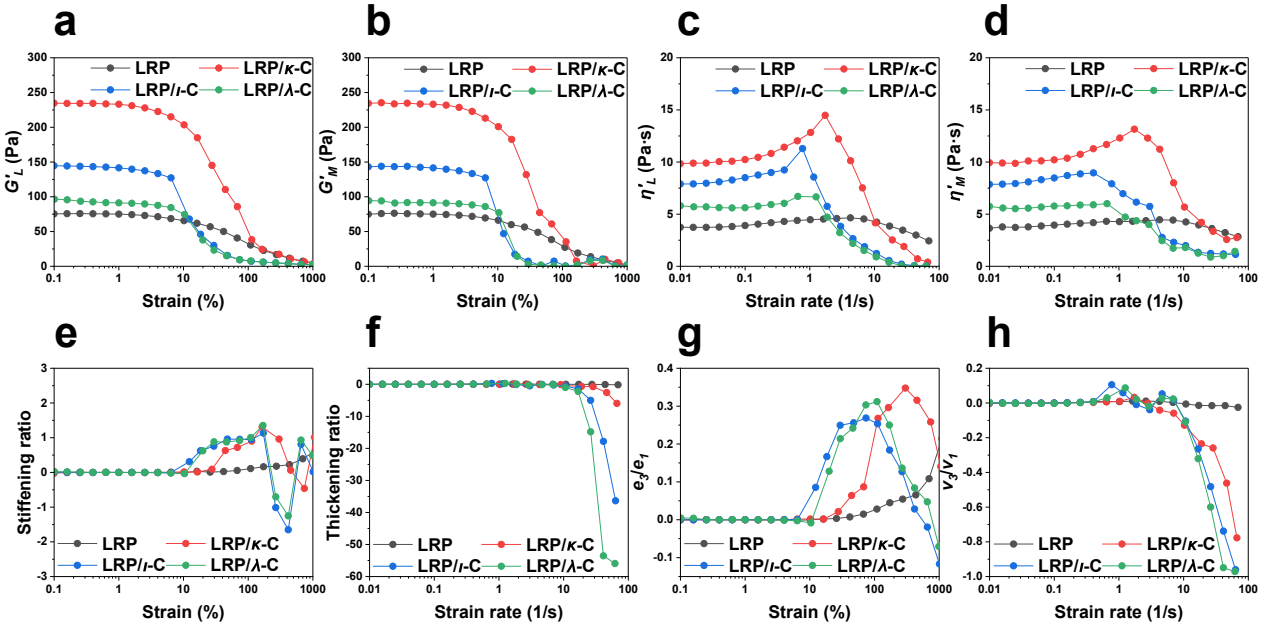

Fig. 4. Nonlinear elastic and viscous LAOS parameters of LRS/carrageenan binary hydrogels: large strain modulus, G'_L (a); minimum strain modulus, G'_M (b); large rate dynamic viscosity, η'_L (c); minimum rate dynamic viscosity, η'_M (d); strain stiffening ratio (e); shear thickening ratio (f); elastic Chebyshev coefficient intensity, e_3/e_1 (g); and viscous Chebyshev coefficient intensity, v_3/v_1 (h).

decreased greatly and then tended to be smooth when the strain was near zero. In particular, G'_M became unstable under more than 100% strain, which might indicate the collapse of the network structure. Compared to LRS/κ-C, the G'_M of LRS/ι-C and LRS/λ-C appeared earlier (approximately 20% strain), corresponding to the results shown in Fig. 2d. This result suggested that the network structure of LRS/κ-C might be superior to those of LRS/ι-C and LRS/λ-C. Moreover, η'_L and η'_M indicate the instantaneous viscosity at the minimum and maximum strain rates, respectively (Ewoldt et al., 2008) (Fig. 4c and d). Both η'_L and η'_M tended to increase and then decrease at strain rates beyond the LRV, corresponding to the weak strain overshoot behavior shown in Fig. 2d. However, the difference in the details between the η'_L and η'_M curves of the binary hydrogels with carrageenan indicated the difference in the intracycle instantaneous viscosity dissipation coefficients under LAOS (Ewoldt et al., 2008). Specifically, binary hydrogels exhibited intracycle shear thickening ($\eta'_L > \eta'_M$) before η'_L reached its apex, followed by intracycle shear thinning ($\eta'_L < \eta'_M$). The order in which the maximum values of η'_L and η'_M occurred was LRS/κ-C > LRS/λ-C > LRS/ι-C, which occurred in the order as in the steady-state flow sweep (Fig. 2b). These results suggested that there was a difference between the viscous and elastic characteristics of the network structure of the LRS/carrageenan binary hydrogels.

The variation trend of the strain-stiffness ratio and shear-thickening ratio under LAOS further revealed the nonlinear viscoelastic behaviors of LRS-based hydrogels (Fig. 4e and f). When the strain exceeded the LVR (> 4%), the stiffness ratio of all the samples began to increase. The intracycle strain-stiffening behaviors (stiffness ratio > 0) of the binary hydrogels with carrageenan were stronger than those of the individual LRS hydrogel. The obvious intracycle strain-stiffening behaviors of LRS/ι-C and LRS/λ-C appeared earlier, indicating that LRS/κ-C was more resistant to external stress. Notably, the stiffness ratio of the LRS/carrageenan binary hydrogels fluctuated in the range of 100%–1000% strain, indicating a rapid transition between intracycle strain stiffening and intracycle strain softening. These results suggested that the binary hydrogel network suffered undesirable shrinkage or damage under large deformation, and its destruction occurred faster than its reconstruction. Moreover, the LRS/carrageenan binary hydrogels exhibited significant intracycle shear thinning with a thickening ratio < 0 at high strain (> 100%). The absolute value of the thickening ratio was related to the intracycle shear thinning strength of the LRS/carrageenan binary hydrogels, which could indicate the structural properties of the hydrogel rearrangement network to some extent. Therefore, the thickening ratio results suggested that the resistance to large deformations of the binary hydrogel network structure followed the order of LRS/κ-C > LRS/ι-C > LRS/λ-C.

In addition, the detailed nonlinear behaviors of the LRS/carrageenan binary hydrogels and individual LRS hydrogel could be understood from the variation trend of the ratios of the third to the first Chebyshev coefficients (e_3/e_1 for elastic and v_3/v_1 for viscous) (Fig. 4g and h). At strains above 4%, the e_3/e_1 of the hydrogel samples was greater than zero, indicating intracycle strain stiffening (Wang & Selomulya, 2022). The contributions of the three carrageenan types to the intracycle strain stiffening of the LRS hydrogel could be identified in more detail according to the order in which the strain began to increase sharply: LRS/κ-C < LRS/λ-C < LRS/ι-C. The network structure of LRS/κ-C was more stable when responding to the change in strain. Moreover, when the strain increased to a certain value, the e_3/e_1 of the binary hydrogels began to decrease in the same order as the increase, suggesting the changes of the intracycle strain stiffening behavior possibly due to the further disruption of the network structure (Erturk, Bonilla, & Kokini, 2021; Niu, Li, Wang, Adhikari, & Chen, 2018). LRS/ι-C and LRS/λ-C exhibited intracycle strain softening at the highest strain. The variation in v_3/v_1 showed a similar trend. The v_3/v_1 values of the LRS/carrageenan binary hydrogels decreased sharply after a short increase. The short rise confirmed the weak strain overshoot behavior, as shown in Fig. 2d. The continuous decrease in v_3/v_1 to a negative value indicated that intracycle shear thinning occurred under the high strain. In this case, the deformed and damaged network structures of the LRS/carrageenan binary hydrogels were more easily aligned with the flow field under large shear. The network structure of LRS/κ-C exhibited stronger shear resistance than LRS/ι-C and LRS/λ-C, which resulted in a weaker response to shear thinning.

3.4. Water distribution of LRS/carrageenan binary hydrogels

Typically, the degree of freedom and distribution of water in a

hydrogel system are determined by its network structure and can be detected rapidly and nondestructively by the LF-NMR technique. For starch-based hydrogels, the lower transverse spin–spin relaxation time (T_2) of hydrogen protons usually indicates the tight binding of water molecules to polysaccharides and the relative decrease in their fluidity (Ma, Zhu, & Wang, 2019). The T_2 relaxation peak vertex times of the individual LRS hydrogel and LRS/carrageenan binary hydrogels are depicted in Table 1. Basically, T_{2b} (0.1–1 ms) and T_{21} (1–10 ms) represent bound water, T_{22} (10–100 ms) corresponds to trapped water in the hydrogel structure, and T_{23} within 100–10,000 ms indicates free water (Jiang et al., 2022). Two common peaks with extreme values in the range of 0.2–0.4 ms and 667.0–1190.2 ms were detected in three LRS/carrageenan binary hydrogels and the individual LRS hydrogel. The T_{23} of LRS was moved forward by 79.8–523.2 ms with the incorporation of carrageenan, and ι-C exhibited the greatest increase. In addition, a T_{21} peak with no significant difference was observed for LRS, LRS/κ-C, and LRS/λ-C, while a distinctive T_{22} peak at 17.69 ms appeared in the T_2 curve of LRS/ι-C. These results suggested that the incorporation of carrageenan improved the ability of LRS hydrogels to immobilize water. Similarly, Ma et al. (2019) reported that the movement of water molecules in corn starch/konjac glucomannan mixture was restricted by the addition of polysaccharides. Luo et al. (2021) reported that *Mesona chinensis* polysaccharides enhanced the structure of the gel network by interacting with starch molecules, thereby reducing the mobility of water protons. Therefore, the LRS/carrageenan binary hydrogels could wrap water with advantages and restrict the free movement of water molecules in the hydrogel network skeleton.

In this section, MRI was used to investigate the spatial distribution of water in the individual LRS hydrogel and LRS/carrageenan hydrogel samples. Typically, brighter and redder pseudo-color images suggest a higher corresponding hydrogen proton density (Jiang et al., 2022). The T_1- and T_2-weighted images and their corresponding relative intensities are displayed in Fig. 5a and b, respectively. In the present work, the T_2-weighted images of all the samples were redder and brighter than the T_1-weighted images, indicating that free water was the majority of the samples, which agreed with the hydrogel characteristics and corresponded to the T_2 relaxation results (Table 1). Moreover, the T_1-weighted image intensities of the LRS/carrageenan binary hydrogels were significantly greater than that of the single LRS carrier ($p < 0.05$), indicating that the amount of immobilized water increased in the hydrogel system in which LRS cooperated with carrageenan. This phenomenon reflected better viscoelasticity of the LRS/carrageenan binary hydrogels (Fig. 2), which was due to the changes in LRS hydrogel network structures by the incorporation of carrageenan (Fig. 1). Similarly, studies on scallop gonads hydrolysates-based and gellan gum/puerarin hydrogels have shown that the increase in immobilized water and viscoelasticity were both the results of network structure development (Xu et al., 2024; Yan, Jiang, Li, Sun, Lai, & Wu, 2023). In particular, LRS/ι-C, exhibited not only a higher signal intensity for immobilized water but also the lowest signal intensity for free water, which corresponded to the T_2 curves and might be attributed to the structural characteristics of the binary hydrogels.

Table 1
Transverse spin–spin relaxation time of LRS/carrageenan binary hydrogels.

Sample	Relaxation time (ms)			
	T_{2b}	T_{21}	T_{22}	T_{23}
LRS	0.24 ± 0.13[a]	7.06 ± 1.25[a]	–	1190.18 ± 48.24[c]
LRS/κ-C	0.37 ± 0.08[a]	6.44 ± 1.12[a]	–	1110.35 ± 45.01[b]
LRS/ι-C	0.26 ± 0.04[a]	–	17.69 ± 1.84[a]	666.99 ± 0.00[a]
LRS/λ-C	0.33 ± 0.09[a]	8.42 ± 0.58[a]	–	1084.37 ± 0.00[b]

Data are expressed as means ± SD from triplicate determinations. Different letters in the same column indicate significant differences ($p < 0.05$). "-", not detectable.

3.5. Thermal characteristics of LRS/carrageenan binary hydrogels

The interaction between starch and nonstarch polysaccharides during heating can be monitored by DSC to obtain the required heat energy, which reflects the difficulty of gelatinization of starch components in the mixed system (Zheng et al., 2021). The gelatinization parameters of the LRS/carrageenan mixtures and individual LRS are displayed in Table 2. For all samples, there was an endothermic peak in the range of 30–110 °C, mainly due to the destruction of the crystal structure during the starch gelatinization process. The thermal transition temperature, including the onset (T_o), peak (T_p), and conclusion (T_c) temperatures, represents the stability of the crystal structure of starch materials (Xie et al., 2021). Although the incorporation of carrageenan had no significant effect on the T_p of LRS, the T_o and T_c of LRS/κ-C moved forward significantly compared with that of the individual LRS, indicating the promotion of gelatinization. A similar phenomenon has also been revealed in the mixed systems of rice starch and four polysaccharides, including high-methoxyl pectin, carboxymethyl cellulose, xanthan gum, and konjac glucomannan (Zheng et al., 2021). Moreover, the ΔH_{gel} values of the three LRS/carrageenan samples decreased by 32.1%-88.4% compared to that of the individual LRS sample, indicating that the addition of carrageenan reduced the energy required for starch gelatinization. The decrease in ΔH_{gel} could be attributed to the interaction between LRS and carrageenan, which altered the coupling forces between the amorphous and crystalline regions. The lowest ΔH_{gel} was obtained from LRS/κ-C, probably due to the insertion of polysaccharide chains into the double helix of starch molecules and the strong intermolecular interactions. The thermal properties further revealed that different types of carrageenan promoted the gelatinization process of LRS, with κ-C being the best, followed by ι-C and λ-C.

3.6. Structural characteristics of LRS/carrageenan binary hydrogels

Raman spectroscopy, XRD, and FTIR were used to analyze the structural information of the binary hydrogels constructed by LRS with three types of carrageenan. The effect of carrageenan on the network development and rheological behaviors of LRS hydrogels could be investigated at the molecular level. Typically, Raman spectroscopy can be applied to detect the internal vibrations of molecules and characterize the degree to which starch materials have ordered structures (Flores-Morales, Jiménez-Estrada, & Mora-Escobedo, 2012; Wang et al., 2016). However, there are currently few reports on the effect of polysaccharides on starch Raman spectroscopy. The incorporation of polysaccharides probably affects the molecular structure stability of starch, as Raman spectroscopy is very sensitive to the fundamental and symmetric vibrations of bonds and less polar molecular groups (Flores-Morales et al., 2012). The signature peak at 480 cm^{-1}, which indicates the structure of the glucose pyranose ring, is very sensitive to changes in starch molecular ordering. In general, the area and full width at half of the maximum (FWHM) of the peak at 480 cm^{-1} were used to characterize the molecular ordering of starch (Wang et al., 2016). The FWHM and area of the peak at 480 cm^{-1} for the LRS/carrageenan binary hydrogels and individual LRS are presented in Table 3. Compared with that of gelatinized LRS alone, the area of the LRS/carrageenan binary hydrogels increased by 47.2%–73.3%, while the FWHM decreased by 8.4%–36.1%. These results suggested that the incorporation of carrageenan improved LRS molecular ordering, as a lower FWHM and larger area of the peak at 480 cm^{-1} indicate greater starch molecular ordering (Wang et al., 2016). Among the binary hydrogels constructed by LRS and three types of carrageenan, the highest degree of starch molecular ordering appeared in LRS/ι-C. Lascombes et al. (2017) suggested that when starch was combined with carrageenan, carrageenan molecules were mainly adsorbed on the surface of starch granules through osmotic pressure, while the phenomenon of electrostatic interactions between endogenous proteins in starch and carrageenan chains was minimal. In addition, during the heating of the starch and carrageenan mixture, the

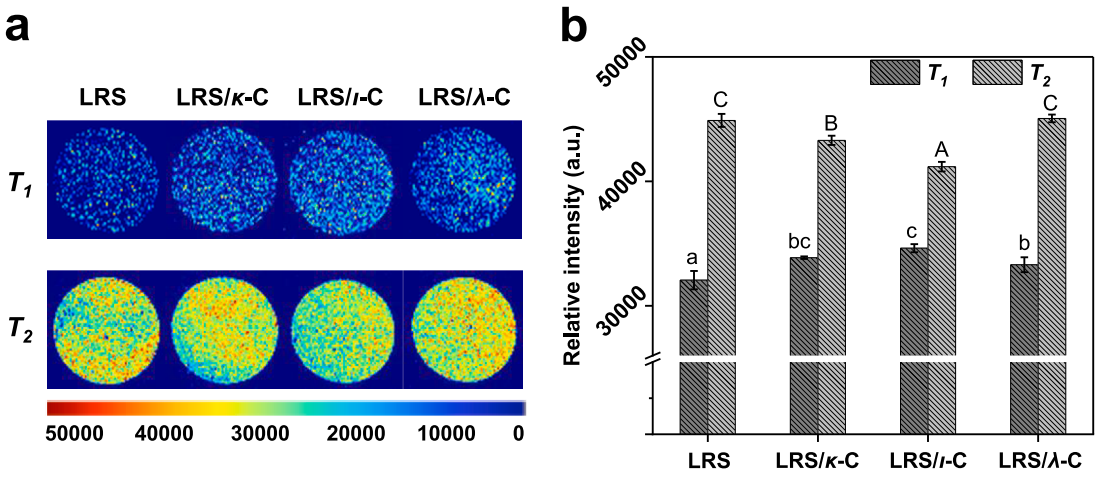

Fig. 5. Magnetic resonance imaging (a) and T_1- and T_2-weighted relative intensities (b) of LRS/carrageenan binary hydrogels. Different lowercase and capital letters indicate significant differences ($p < 0.05$) in the T_1- and T_2-weighted relative intensities, respectively.

Table 2
Thermal characteristics of LRS/carrageenan binary mixtures.

Sample	T_o (°C)	T_p (°C)	T_c (°C)	ΔH_{gel} (J/g)
LRS	55.1 ± 0.38^b	61.46 ± 0.15^a	84.90 ± 1.50^b	16.50 ± 0.05^d
LRS/κ-C	50.98 ± 0.73^a	60.89 ± 1.12^a	72.36 ± 2.00^a	1.91 ± 0.18^a
LRS/ι-C	55.82 ± 1.23^b	62.66 ± 0.12^a	76.97 ± 4.80^a	4.15 ± 0.60^b
LRS/λ-C	54.95 ± 0.37^b	62.49 ± 0.22^a	82.74 ± 0.22^b	11.21 ± 0.60^c

Data are reported as means ± SD from triplicate determinations. Different letters in the same column indicate significant differences ($p < 0.05$). T_o, T_p and T_c represent the onset, peak and conclusion temperatures, respectively, and ΔH_{gel} is the enthalpy for gelatinization.

Table 3
Structural characteristic parameters of LRS/carrageenan binary hydrogels.

Sample	Area of the Raman band at 480 cm^{-1}	FWHM$_{480}$ (cm^{-1})	RC (%)	$R_{1045/1022}$ ratio	$R_{1022/995}$ ratio
LRS	1.80 ± 0.07^a	50.27 ± 1.85^d	0.94 ± 0.04^a	0.55 ± 0.03^a	1.33 ± 0.02^b
LRS/κ-C	2.65 ± 0.08^b	46.03 ± 1.25^c	1.64 ± 0.10^b	0.78 ± 0.01^b	1.36 ± 0.02^c
LRS/ι-C	3.12 ± 0.06^d	32.13 ± 0.38^a	4.05 ± 0.08^c	0.74 ± 0.01^b	1.33 ± 0.01^b
LRS/λ-C	2.82 ± 0.01^c	37.38 ± 0.11^b	3.81 ± 0.18^c	0.76 ± 0.01^b	1.26 ± 0.01^a

Data are reported as means ± SD from triplicate determinations. Different letters in the same column indicate significant differences ($p < 0.05$). FWHM$_{480}$, full-width at the half of the maximum at 480 cm^{-1} Raman band; RC, relative crystallinity.

polysaccharide molecular chains were adsorbed on swollen starch granules with their respective coil conformations (Huc et al., 2014; Matignon et al., 2014). Therefore, it is speculated that the coil conformation of the ι-C molecular chains has a more positive effect on the degree of molecular arrangement and order of LRS than that of λ-C and κ-C. As a result, the LRS/ι-C binary hydrogel exhibited a lower apparent viscosity as shear progressed (Fig. 2b) and a better ability to trap water (Table 1 and Fig. 5). In addition, the sequence of the intersection of G' and G'' under LAOS could also be explained (Fig. 2d).

The long-range structural ordering of starch materials has commonly been investigated by XRD techniques. The characteristic diffraction pattern of starch was lost, and only one broad peak remained for the LRS/carrageenan binary hydrogel freeze-dried samples, which meant that the crystalline structure of starch almost disappeared after being mixed with polysaccharide and gelatinized (data not shown). Moreover, the LRS/carrageenan binary hydrogel samples maintained a relative crystallinity (RC) of less than 5%, as shown in Table 3, which was similar to a previous report on starch/polysaccharide systems (Tu, Adhikari, Brennan, Cheng, Bai, & Brennan, 2023). In the LRS/carrageenan binary hydrogel systems, κ-C, ι-C, and λ-C resulted in RC of 1.6%, 4.1%, and 3.8%, respectively. These results suggested that the degree of long-range ordering of the starch molecular structure in binary hydrogels with ι-C or λ-C was greater than that of LRS/κ-C. Huc et al. (2014) reported that the amount of κ-C captured by starch particles during the gelatinization process was greater than that of ι-C, which was mainly related to molecular chain flexibility and coil conformation, while the carrageenan charge did not seem to be an important parameter. The increase in the number of hydrogen bonds between κ-C and LRS might be a reasonable explanation for preventing the formation of long-range ordered structures during starch retrogradation. Similar findings were reported for the jicama starch/jicama nonstarch polysaccharide system (Huang, Yu, Wang, & Shi, 2023). In addition, the RC and Raman spectra corroborated each other, reflecting the difference in molecular structure order in the LRS/carrageenan binary hydrogel system caused by different types of carrageenan.

Infrared spectroscopy can not only be applied in studying molecular interactions distinguished by changes in absorption bands but is also widely used for the analysis of short-range ordering of starch structures (Wang et al., 2016). The FTIR spectral band in the region of 1200–1000 cm^{-1} corresponds to the stretching vibration of C—O—C, and its intensity can reflect the conformational changes and hydration of processed starch (Xie Zhang, Xia, & Ai, 2020). The orientation of the intermolecular hydrogen bonding of CH and CH_2 in CH_2OH can be characterized by the intensity of the peak at 1022 cm^{-1}, reflecting the characteristics of the amorphous region of starch (Flores-Morales et al., 2012). The short-range ordering obtained from FTIR was mainly related to the presence of double helices in the amorphous and crystalline regions of starch granules, which was different from the long-range ordering obtained from XRD. The extent of the short-range ordered structure of starch could be quantified by the absorbance ratio (1045/1022 cm^{-1}) of deconvoluted FTIR spectral peaks, and 1022/995 cm^{-1} was related to the ratio of amorphous to ordered structures (Sevenou, Hill, Farhat, & Mitchell, 2002). The calculated $R_{1045/1022}$ and $R_{1022/995}$ values are listed in Table 3. The incorporation of carrageenan significantly increased the $R_{1045/1022}$ value of individual LRS, indicating greater short-range molecular ordering. The $R_{1045/1022}$ values of the three binary hydrogel samples were only slightly different but did not significantly differ. There was a significant difference between the $R_{1022/995}$ value of binary hydrogel samples: LRS/κ-C > LRS/ι-C > LRS/λ-C. The presence of carrageenan might lead to increased entanglement

between starch molecules and linear polysaccharide molecules (Xie et al., 2020). Moreover, the flexibility and helical conformation of different types of carrageenan molecular chains might be the main influencing factors (Huc et al., 2014). In the process of co-heating with starch, the helical conformation of carrageenan probably experienced distortion. Previous studies have shown that κ-C and ι-C undergo varying degrees of coil-helix transition in aqueous solutions, while λ-C remains in a coiled state (Schefer et al., 2014). Therefore, the difference in the number and proportion of flexible coil chains and the rigid helices of the three carrageenan molecules might be the decisive reason for the different intermolecular interactions in the LRS/carrageenan binary hydrogels.

In the current work, inferences could be made based on the DSC, Raman spectroscopy, XRD, and FTIR results (Table 2 and Table 3). Carrageenan molecular chains were adsorbed on the surface of starch granules in random coils (Huc et al., 2014; Matignon et al., 2014). During the subsequent mixed heating process, partial self-assembly occurred between the carrageenan and starch molecular chains. At the same time, κ-C and ι-C underwent an autonomous coil-helix conformational transition, while λ-C remained in a random coil state. Therefore, the LRS/carrageenan binary hydrogels exhibited a diverse network structure (Fig. 1), which accurately reflected the linear and nonlinear viscoelasticity (Fig. 2, Fig. 3, and Fig. 4) and the ability to immobilize water (Table 1 and Fig. 5).

4. Conclusions

Carrageenan promoted the interpenetration of binary hydrogel networks, resulting in easier gelatinization of LRS and greater ability to trap water in microstructure. The incorporation of carrageenan reduced the stress resistance of LRS-based hydrogels under large deformations, which was conducive to oral processing and swallowing. Moreover, κ-C promoted the better viscoelasticity of LRS hydrogel, while ι-C was more favorable to the immobilization of water in the hydrogel, which were related to the molecular ordering of the binary hydrogels: LRS/κ-C $<$ LRS/λ-C $<$ LRS/ι-C. This study indicates the nonlinear rheological behaviors and structural characteristics of LRS/carrageenan hydrogels, providing a theoretical basis for the application of LRS hydrogel matrices for dysphagia management.

CRediT authorship contribution statement

Xin-Yu Jiang: Writing – original draft, Validation, Methodology, Investigation, Formal analysis, Data curation, Conceptualization. **Lin Li:** Methodology, Investigation. **Jia-Nan Yan:** Supervision. **Ce Wang:** Supervision. **Bin Lai:** Writing – review & editing, Supervision. **Hai-Tao Wu:** Writing – review & editing, Supervision, Project administration, Funding acquisition.

Declaration of competing interest

The authors declare that they have no known competing financial interests or personal relationships that could have appeared to influence the work reported in this paper.

Data availability

Data will be made available on request.

Acknowledgments

This work was supported by the Science and Technology Program of Liaoning Province (2022JH1/10900010).

References

Cichero, J. A. Y., Lam, P., Steele, C. M., Hanson, B., Chen, J., Dantas, R. O., … Stanschus, S. (2017). Development of international terminology and definitions for texture-modified foods and thickened fluids used in dysphagia management: The IDDSI framework. *Dysphagia, 32*(2), 293–314. https://doi.org/10.1007/s00455-016-9758-y

Duvarci, O. C., Yazar, G., & Kokini, J. L. (2017). The comparison of LAOS behavior of structured food materials (suspensions, emulsions and elastic networks). *Trends in Food Science & Technology, 60*, 2–11. https://doi.org/10.1016/j.tifs.2016.08.014

Erturk, M. Y., Bonilla, J. C., & Kokini, J. (2021). Relationship of non-linear rheological properties and quantitative network analysis parameters as a function of increasingly large amplitude deformations in non-fat, low-fat and high-fat yogurt products. *Food Hydrocolloids, 111*, Article 106194. https://doi.org/10.1016/j.foodhyd.2020.106194

Ewoldt, R. H., Hosoi, A. E., & McKinley, G. H. (2008). New measures for characterizing nonlinear viscoelasticity in large amplitude oscillatory shear. *Journal of Rheology, 52*(6), 1427–1458. https://doi.org/10.1122/1.2970095

Ewoldt, R. H., Winter, P., Maxey, J., & McKinley, G. H. (2010). Large amplitude oscillatory shear of pseudoplastic and elastoviscoplastic materials. *Rheologica Acta, 49*(2), 191–212. https://doi.org/10.1007/s00397-009-0403-7

Flores-Morales, A., Jiménez-Estrada, M., & Mora-Escobedo, R. (2012). Determination of the structural changes by FT-IR, Raman, and CP/MAS 13C NMR spectroscopy on retrograded starch of maize tortillas. *Carbohydrate Polymers, 87*(1), 61–68. https://doi.org/10.1016/j.carbpol.2011.07.011

Gürkan Polat, T., Duman, O., & Tunç, S. (2020). Preparation and characterization of environmentally friendly agar/κ-carrageenan/montmorillonite nanocomposite hydrogels. *Colloids and Surfaces A: Physicochemical and Engineering Aspects, 602*, Article 124987. https://doi.org/10.1016/j.colsurfa.2020.124987

Huang, J., Yu, M., Wang, S., & Shi, X. (2023). Effects of jicama (*Pachyrhizus erosus* L.) non-starch polysaccharides with different molecular weights on structural and physicochemical properties of jicama starch. *Food Hydrocolloids, 139*, Article 108502. https://doi.org/10.1016/j.foodhyd.2023.108502

Huc, D., Matignon, A., Barey, P., Desprairies, M., Mauduit, S., Sieffermann, J. M., & Michon, C. (2014). Interactions between modified starch and carrageenan during pasting. *Food Hydrocolloids, 36*, 355–361. https://doi.org/10.1016/j.foodhyd.2013.08.023

Hyun, K., Wilhelm, M., Klein, C. O., Cho, K. S., Nam, J. G., Ahn, K. H., … McKinley, G. H. (2011). A review of nonlinear oscillatory shear tests: Analysis and application of large amplitude oscillatory shear (LAOS). *Progress in Polymer Science, 36*(12), 1697–1753. https://doi.org/10.1016/j.progpolymsci.2011.02.002

Jia, S., Tao, H., Zhao, H., Yu, B., Wu, Z., Liu, P., & Cui, B. (2023). Effects of *Lycium barbarum* polysaccharide on pasting, rheology, and *in vitro* digestibility of starch. *Starch - Stärke, 75*(1–2), Article 2200185. https://doi.org/10.1002/star.202200185

Jiang, X., Gu, Y., Zhang, L., Sun, J., Yan, J., Wang, C., … Wu, H. (2023). Physicochemical properties of granular and gelatinized lotus rhizome starch with varied proximate compositions and structural characteristics. *Foods, 12*(23), Article 23. https://doi.org/10.3390/foods12234330

Jiang, X.-Y., Yan, J.-N., Li, L., Sun, W., Nie, B., & Wu, H.-T. (2022). Gel properties and interactions of scallop (*Patinopecten yessoensis*) male gonad hydrolysates and nonionic polysaccharide mixtures. *Food Chemistry, 394*, Article 133482. https://doi.org/10.1016/j.foodchem.2022.133482

Kim, H.-S., Patel, B., & BeMiller, J. N. (2013). Effects of the amylose–amylopectin ratio on starch–hydrocolloid interactions. *Carbohydrate Polymers, 98*(2), 1438–1448. https://doi.org/10.1016/j.carbpol.2013.07.035

Kong, D., Zhang, M., Mujumdar, A. S., & Li, J. (2023). Feasibility of hydrocolloid addition for 3D printing of Qingtuan with red bean filling as a dysphagia food. *Food Research International, 165*, Article 112469. https://doi.org/10.1016/j.foodres.2023.112469

Lascombes, C., Agoda-Tandjawa, G., Boulenguer, P., Le Garnec, C., Gilles, M., Mauduit, S., … Langendorff, V. (2017). Starch-carrageenan interactions in aqueous media: Role of each polysaccharide chemical and macromolecular characteristics. *Food Hydrocolloids, 66*, 176–189. https://doi.org/10.1016/j.foodhyd.2016.11.025

Lin, J.-H., Liang, C.-W., & Chang, Y.-H. (2016). Effect of starch source on gel properties of kappa-carrageenan-starch dispersions. *Food Hydrocolloids, 60*, 509–515. https://doi.org/10.1016/j.foodhyd.2016.04.024

Liu, B., Zhu, S., Zhong, F., Yokoyama, W., Huang, D., & Li, Y. (2021). Modulating storage stability of binary gel by adjusting the ratios of starch and kappa-carrageenan. *Carbohydrate Polymers, 268*, Article 118264. https://doi.org/10.1016/j.carbpol.2021.118264

Liu, D., Li, Z., Fan, Z., Zhang, X., & Zhong, G. (2019). Effect of soybean soluble polysaccharide on the pasting, gels, and rheological properties of kudzu and lotus starches. *Food Hydrocolloids, 89*, 443–452. https://doi.org/10.1016/j.foodhyd.2018.11.003

Luo, Y., Han, X., Shen, M., Yang, J., Ren, Y., & Xie, J. (2021). *Mesona chinensis* polysaccharide on the thermal, structural and digestibility properties of waxy and normal maize starches. *Food Hydrocolloids, 112*, Article 106317. https://doi.org/10.1016/j.foodhyd.2020.106317

Ma, S., Zhu, P., & Wang, M. (2019). Effects of konjac glucomannan on pasting and rheological properties of corn starch. *Food Hydrocolloids, 89*, 234–240. https://doi.org/10.1016/j.foodhyd.2018.10.045

Matignon, A., Barey, P., Desprairies, M., Mauduit, S., Sieffermann, J. M., & Michon, C. (2014). Starch/carrageenan mixed systems: Penetration in, adsorption on or exclusion of carrageenan chains by granules? *Food Hydrocolloids, 35*, 597–605. https://doi.org/10.1016/j.foodhyd.2013.07.028

Min, C., Zhang, C., Cao, Y., Li, H., Pu, H., Huang, J., & Xiong, Y. L. (2023). Rheological, textural, and water-immobilizing properties of mung bean starch and flaxseed protein composite gels as potential dysphagia food: The effect of Astragalus polysaccharide. *International Journal of Biological Macromolecules, 239*, Article 124236. https://doi.org/10.1016/j.ijbiomac.2023.124236

Necas, J., & Bartosikova, L. (2013). Carrageenan: A review. *Veterinární Medicína, 58*(4), 187–205. https://doi.org/10.17221/6758-VETMED

Niu, J., Li, D., Wang, L., Adhikari, B., & Chen, X. D. (2018). Synthesis of carboxymethyl flaxseed gum and study of nonlinear rheological properties of its solutions. *International Journal of Food Engineering, 14*(1), 20170185. https://doi.org/10.1515/ijfe-2017-0185

Rochas, C., Rinaudo, M., & Vincendon, M. (1980). Structural and conformational investigation of carrageenans. *Biopolymers, 19*(12), 2165–2175. https://doi.org/10.1002/bip.1980.360191203

Schefer, L., Adamcik, J., & Mezzenga, R. (2014). Unravelling secondary structure changes on individual anionic polysaccharide chains by atomic force microscopy. *Angewandte Chemie International Edition in English, 53*(21), 5376–5379. https://doi.org/10.1002/anie.201402855

Sevenou, O., Hill, S. E., Farhat, I. A., & Mitchell, J. R. (2002). Organisation of the external region of the starch granule as determined by infrared spectroscopy. *International Journal of Biological Macromolecules, 31*(1–3), 79–85. https://doi.org/10.1016/S0141-8130(02)00067-3

Song, J., Rong, L., Li, J., Shen, M., Yu, Q., Chen, Y., … Xie, J. (2024). Effects of three different polysaccharides on the sol gel-behavior, rheological, and structural properties of tapioca starch. *International Journal of Biological Macromolecules, 254*, Article 128053. https://doi.org/10.1016/j.ijbiomac.2023.128053

Su, C., Li, D., Wang, L., & Wang, Y. (2023). Green double crosslinked starch-alginate hydrogel regulated by sustained calcium ion-gluconolactone release for human motion monitoring. *Chemical Engineering Journal, 455*, Article 140653. https://doi.org/10.1016/j.cej.2022.140653

Tu, J., Adhikari, B., Brennan, M. A., Cheng, P., Bai, W., & Brennan, C. S. (2023). Interactions between sorghum starch and mushroom polysaccharides and their effects on starch gelatinization and digestion. *Food Hydrocolloids, 139*, Article 108504. https://doi.org/10.1016/j.foodhyd.2023.108504

Turksoy, S., Erturk, M. Y., Bonilla, J., Turasan, H., & Kokini, J. L. (2020). Effect of aging at different temperatures on LAOS properties and secondary protein structure of hard wheat flour dough. *Journal of Cereal Science, 92*, Article 102926. https://doi.org/10.1016/j.jcs.2020.102926

Wang, S., Sun, Y., Wang, J., Wang, S., & Copeland, L. (2016). Molecular disassembly of rice and lotus starches during thermal processing and its effect on starch digestibility. *Food & Function, 7*(2), 1188–1195. https://doi.org/10.1039/C6FO00067C

Wang, Y., & Selomulya, C. (2022). Food rheology applications of large amplitude oscillation shear (LAOS). *Trends in Food Science & Technology, 127*, 221–244. https://doi.org/10.1016/j.tifs.2022.05.018

Wang, Z., Zhong, Z., Zheng, B., Zhang, Y., & Zeng, H. (2023). Effects of *Porphyra haitanensis* polysaccharides on gelatinization and gelatinization kinetics of starches with different crystal types. *International Journal of Biological Macromolecules, 242*, Article 125117. https://doi.org/10.1016/j.ijbiomac.2023.125117

Wei, Z., Ou, Y., Lan, X., Tang, J., & Zheng, B. (2023). Effects of laminarin on the structural properties and *in vitro* digestion of wheat starch and its application in noodles. *LWT - Food Science and Technology, 178*, Article 114543. https://doi.org/10.1016/j.lwt.2023.114543

Xie, F., Zhang, H., Xia, Y., & Ai, L. (2020). Effects of tamarind seed polysaccharide on gelatinization, rheological, and structural properties of corn starch with different amylose/amylopectin ratios. *Food Hydrocolloids, 105*, Article 105854. https://doi.org/10.1016/j.foodhyd.2020.105854

Xie, J., Ren, Y., Xiao, Y., Luo, Y., & Shen, M. (2021). Interactions between tapioca starch and *Mesona chinensis* polysaccharide: Effects of urea and NaCl. *Food Hydrocolloids, 111*, Article 106268. https://doi.org/10.1016/j.foodhyd.2020.106268

Xu, S.-Q., Du, Y.-N., Zhang, Z.-J., Yan, J.-N., Sun, J.-J., Zhang, L.-C., … Wu, H.-T. (2024). Gel properties and interactions of hydrogels constructed with low acyl gellan gum and puerarin. *Carbohydrate Polymers, 326*, Article 121594. https://doi.org/10.1016/j.carbpol.2023.121594

Yan, J.-N., Jiang, X.-Y., Li, L., Sun, W., Lai, B., & Wu, H.-T. (2023). Storage stability of scallop (*Patinopecten yessoensis*) male gonad hydrolysates/κ-carrageenan composite hydrogels embeded curcumin. *Food Hydrocolloids, 136*, Article 108228. https://doi.org/10.1016/j.foodhyd.2022.108228

Seighalani, Z. B., Joyner, H., & Ross, C. (2020). Relationships among rheological, sensory, and wear behaviors of cheeses. *Journal of Texture Studies, 51*(5), 702–721. https://doi.org/10.1111/jtxs.12547

Zheng, J., Huang, S., Zhao, R., Wang, N., Kan, J., & Zhang, F. (2021). Effect of four viscous soluble dietary fibers on the physicochemical, structural properties, and *in vitro* digestibility of rice starch: A comparison study. *Food Chemistry, 362*, Article 130181. https://doi.org/10.1016/j.foodchem.2021.130181

Zheng, J., Liu, M., Zhang, M., Kan, J., & Zhang, F. (2019). Effects of pectin on the pasting, rheological, and textural properties of lotus root starch. *Starch - Stärke, 71*(3–4), 1700347. https://doi.org/10.1002/star.201700347

Zheng, J., Wang, N., Yang, J., You, Y., Zhang, F., Kan, J., & Wu, L. (2024). New insights into the interaction between bamboo shoot polysaccharides and lotus root starch during gelatinization, retrogradation, and digestion of starch. *International Journal of Biological Macromolecules, 254*, Article 127877. https://doi.org/10.1016/j.ijbiomac.2023.127877

Zhong, G., Chen, Z. D., & We, Y. M. (2007). Physicochemical properties of lotus (*Nelumbo nucifera* Gaertn.) and kudzu (*Pueraria hirsute* Matsum.) starches. *International Journal of Food Science & Technology, 42*(12), 1449–1455. https://doi.org/10.1111/j.1365-2621.2006.01363.x

Zhu, F. (2017). Structures, properties, and applications of lotus starches. *Food Hydrocolloids, 63*, 332–348. https://doi.org/10.1016/j.foodhyd.2016.08.034